FUNCTIONAL MAGNETIC RESONANCE IMAGING OF THE SPINAL CORD IN PAINFUL DIABETIC NEUROPATHY

BY
CHERYL JONES

Supervisor: Dr. K.L. Malisza

A thesis submitted in partial fulfillment
of the Honours Thesis (05.4111/6) Course

Department of Biology
University of Winnipeg
2008

ABSTRACT

Diabetic neuropathy, a secondary complication of diabetes mellitus, is often first characterized by allodynia, hyperalgesia, or spontaneous pain. The mechanism by which diabetes alters pain transmission is not well understood, but recent evidence suggests spinal cord involvement. Behavioural studies have shown that streptozotocin (STZ) induced diabetic rats exhibit hyperalgesia. Functional magnetic resonance imaging (fMRI) was used to compare activity in the spinal cord upon noxious electrical stimulation (15 V, 0.3 ms, 0.3 Hz) of the hind paw in STZ-induced diabetic and control rats (7–8 mA). Experiments were conducted on rats one month following STZ injection (n=4) and healthy age-matched controls (n=4). Diabetic rats were smaller, hyperglycaemic, and had lower blood pH than control animals. FMRI activity at the lumbar enlargement of the spinal cord was observed in both control and diabetic animals in the dorsal horn ipsilateral to stimulus. Control animals exhibited greater fMRI activity in the contralateral dorsal horn, and ipsilateral and contralateral ventral horn, and had a higher percentage signal change compared to diabetic rats. The results of this study are consistent with reports that primary afferent input to the spinal cord is diminished by diabetes, and suggest fMRI may be useful in early detection of diabetic neuropathy.

ACKNOWLEDGMENTS

I would like to first thank my mentor and supervisor Dr. Malisza for her guidance, encouragement, and remarkable patience in answering my never-ending stream of questions, throughout this project. It has been an honour to work with her.

I would also like to thank Dr. Fernyhough and the staff at the St. Boniface Research Centre for providing and caring for the animals used in this project, as well as Dr. Calcutt at the University of California San Diego for answering my many questions and providing valuable feedback.

At the National Research Council Institute for Biodiagnostics I thank surgical staff for performing the surgery and animal monitoring, and Dr. Gruwel for putting in a lot of time showing me the ropes in image acquisition and for his patience and sense of humour throughout the experiments. I would also like to thank Dr. Summers for help with statistics, Brendan Matwiy and Derek Foreman for technical support, and Dr. Shiloff for her continuous encouragement and moral support. Also, thank you to the Manitoba Institute of Child Health for providing funding to help me complete this project.

Lastly, I would like to thank my committee members; Dr. Peeling and Dr. Wiegand, aswell as the thesis course coordinator, Dr. Moodie, for their feedback and advice.

TABLE OF CONTENTS

ABSTRACT ..... **ii**

ACKNOWLEDGMENTS ..... **iii**

TABLE OF CONTENTS ..... **iv**

I. LIST OF TABLES ..... **v**

II. LIST OF FIGURES ..... **vi**

II. LIST OF FIGURES ..... **vi**

III. INTRODUCTION **1**

III.1. Rationale for the present study 1
III.2. Diabetic neuropathy 1
III.3. Animal Models of Diabetes 3
III.4. General structure of the rat spinal cord 5
III.5. Noxious stimulation of the hind limb 6
III.6. The hemodynamic response 7
III.7. Magnetic Resonance Imaging 7
III.8. Functional Magnetic Resonance Imaging 9

IV METHODS **12**

IV.1. Animal preparation 12
IV.2. Data acquisition 13
IV.3. Data analysis 16

V. RESULTS **17**

V.1. Time course data 18
V.2. Location of fMRI activity 20

VI. DISCUSSION **23**

VII CONCLUSIONS **31**

VIII REFERENCES **32**

I. LIST OF TABLES

Table 1. Mean weight and some measured physiological parameters of the blood obtained during fMRI experiments in diabetic and control rats. (Mean ± SD).....18

II. LIST OF FIGURES

Figure 1. Schematic drawing of the lumbar spinal cord.....6

Figure 2. Anatomical image to identify lumbar spinal cord segments.....14

Figure 3. Stimulation paradigm.....15

Figure 4. Averaged time courses of diabetic (n=4) and control (n=4) animals in response to noxious electrical stimulation. (mean ± SEM).....19

Figure 5. Mean signal intensity changes (mean ± SEM) across control (n=4, pink) and diabetic animals (n=4, blue) in each active stimulation period.....20

Figure 6. MRI activation map in control animals following noxious electrical stimulation of the right hind paw. 21

Figure 7. fMRI activation map in diabetic animals following noxious electrical stimulation of the right hind paw 22

Figure 8. Overlay of combined fMRI activations 22

III. INTRODUCTION

III.1. Rationale for the present study

According to the World Health Organization, there will be a predicted 300 million sufferers of diabetes mellitus by the year 2025 (1998). The increased incidence of diabetes will also see a rise in complications secondary to diabetes, such as retinopathy, nephropathy, and neuropathy. This will translate to increased health care costs, in addition to causing a great amount of misery to patients. There are currently no treatment options that either stop or reverse the progress of diabetic neuropathy (Scott and Tesfaye, 2001) although institution and maintenance of glycemic control can slow its progression. It is therefore important to be able to predict early on which patients are at risk for developing, or are in early asymptomatic stages of, diabetic neuropathy for treatment options to be most effective. In the future, we hope to be able to assess the potential for spinal cord functional magnetic resonance imaging (fMRI) to detect early stages of diabetic neuropathy. The aim of this study was to determine if differences exist in fMRI activation in the spinal cord of one month diabetic rats compared to age-matched healthy control animals.

III.2. Diabetic neuropathy

Diabetic neuropathy is a secondary complication of diabetes mellitus. Diabetes can be divided into two main groups, type I and type II. Type I diabetes, formerly called insulin-dependent, or juvenile diabetes, is caused by the pancreas being unable to produce enough insulin to prevent hyperglycemia. In type II diabetes, hyperglycemia is caused by

the target tissues becoming resistant to insulin. Although type II diabetes typically has a later age of onset, increased incidence is noticed in children, including obese adolescents. Both types of diabetes give rise to a number of secondary complications, including neuropathy. Diabetic neuropathy typically targets the long sensory nerves of the arms and legs first, affecting sensation in the hands and feet. Lack of sensation can lead to infection going unnoticed, which necessitates, in the worst cases, limb amputation.

Approximately 10% to 20% of patients with diabetic neuropathy experience extreme pain, which can be occasional, spontaneous, persistent, touch-evoked (allodynia), or a hypersensitivity to a mildly noxious stimulus (hyperalgesia)(Cesena and Calcutt, 1999). Medications commonly prescribed for pain are ineffective in treating diabetic neuropathy, and the side effects often outweigh the benefits (reviewed in Scott and Tesfaye, 2001).

While the mechanism by which diabetic neuropathy alters pain perception is not well understood, recent evidence suggests spinal cord involvement (Freshwater *et al*, 2002; Selvarajah *et al*, 2006; Calcutt and Chaplan, 1997; Honda *et al*, 2007; Ramos *et al*, 2007). For instance, in clinical diabetes, a reduction in spinal cord area can be detected in sub-clinical diabetic neuropathy (Selvarajah *et al*, 2006). In animal models of diabetic neuropathy, cyclooxygenase-2 protein levels were elevated in the spinal cord, and prostaglandin E2 release upon noxious stimulation was prolonged in the spinal cord while hyperalgesia following the noxious stimulus can be alleviated by a spinally delivered cyclooxygenase inhibitor (Freshwater *et al*., 2002). Aldose reductase inhibitors (ARIs)

have been effective in alleviating hyperalgesia in experimental diabetes (Tomlinson *et al*., 1982). Treatment of diabetic rats with an ARI that does not penetrate the spinal cord, however, has no effect on the level of hyperalgesia in response to formalin injection even though function in the peripheral nerve was protected (Ramos *et al*., 2007). This indicates that glucose metabolism within the spinal cord itself may be important in mediating hyperalgesia. Furthermore, Honda *et al*. (2007) found that the spinal cord of diabetic mice had increased activity of Ca^{2+}-dependent protein kinase C which, the authors suggest, is involved in the development of hyperalgesia and allodynia by abnormally activating sensory neurons in laminae II and III of the spinal cord.

III.3. Animal Models of Diabetes

Animal models are useful in studying diabetes, since they share similar precursors to nerve degeneration as human diabetic patients. There are several rodent models of diabetes that are used in studying diabetic neuropathy, including gene-prone and chemically induced mouse and rat models. Given the small spinal cord of the mouse, it would be difficult to perform spinal fMRI on these animals. In addition, spinal fMRI in the rat is well established in our laboratory (Malisza *et al*., 2003; Lawrence *et al*., 2004; 2007; 2008). The two common type I rat models of diabetic neuropathy include the gene-prone Biobreeding/Worcester (BB/Wor-DP) rats, and streptozotocin(STZ)-induced rats, and a common model of type II diabetes is the Zucker diabetic fatty (ZDF) rat (reviewed in Gabra *et al*., 2006). Although the level of hyperalgesia in ZDF rats stabilizes at 13 weeks of age, these rats are obese and much too large to image with the available experimental setup. Of the two common type I models of diabetic neuropathy, the STZ-

induced diabetic rat is preferred for this study because the onset of diabetes can be controlled, it is less costly, and the level of hyperalgesia, which develops at the same time as hyperglycemia, stabilizes over 1 to 4 weeks after injection (Gabra *et al*., 2006) and persists for several weeks. In this model, type I diabetes is induced in rats by a single injection of streptozotocin (STZ), which makes the pancreas unable to produce insulin. STZ-induced diabetic rats display slowed conduction of action potentials in peripheral nerve trunks (Tomlinson *et al.*, 1982), deficient neurotrophic support from target cell derived neurotrophins (Fernyhough *et al.*, 1995), impaired axonal regeneration after a nerve crush (Ekstrom and Tomlinson, 1989), and development of tactile allodynia (Calcutt and Chaplan, 1997) and hyperalgesia (Gabra *et al*., 2006). These functional changes can be measured in diabetic rats of this model. The changes are comparable to those observed in diabetic patients and are clear markers for early to late stage neuropathy.

Although fMRI is often used to examine neuronal activity in the brain, it has also been used in studies of the spinal cord of both animals and humans (Malisza *et al*, 2003; Lawrence *et al*, 2004; 2007; 2008; Majcher *et al*., 2006) and this knowledge is extended to determine fMRI activity in the lumbar spinal cord of STZ-induced diabetic rats in response to painful electrical stimuli. Before explaining the basis for the signal obtained in fMRI, it is useful to first look at the structure of the spinal cord and the response to painful electrical stimulation of the hind limb in the rat.

III.4. General structure of the rat spinal cord

The spinal cord is a part of the central nervous system that functions in relaying messages between the peripheral nervous system and the brain. It is surrounded by cerebral spinal fluid (CSF) and protected by bony vertebrae. The rat spinal cord can be divided into 34 segments including 8 cervical, 13 thoracic, 6 lumbar, 4 sacral, and 3 coccygeal (Hebel and Stromberg, 1986), from each of which project anterior and posterior spinal nerves that form part of the peripheral nervous system. Bundles, or tracts, of axons that can be myelinated or unmyelinated are located in the peripheral white matter of the spinal cord. The interior grey matter of the spinal cord contains neuroglia, cell bodies and their dendrites and axons (Mizisin *et al.*, 2006; Squire *et al*., 2003). The grey matter appears butterfly-shaped, and can be subdivided into groups known as laminae of Rexed (see Figure 1). The posterior part of the grey matter, also known as the dorsal horn, contains laminae I-VI which receive somatosensory information from afferent neurons, such as pain, pressure and temperature (Squire *et al*., 2003). Laminae VII to IX make up the anterior, or ventral horn, region of the grey matter, and lamina X is located in the centre of the grey matter. Laminae IX and X contain motor neurons that exit the ventral roots to supply information to muscles (Squire *et al*., 2003). Laminae V to VIII are sometimes referred to as the intermediate horn, and contain many interneurons whose axons stay within the spinal cord and are involved in proprioceptive (movement, muscle tone, body position) information transfer in the CNS (Squire *et al*., 2003). The lumbar enlargement of the spinal cord, where the size of the grey matter is much larger, contains many sensory and motor neurons that control sensations from, and movement in, the hind limbs.

III.5. Noxious stimulation of the hind limb

Upon painful stimulation, nociceptive information is relayed from nociceptors on the skin to the central nervous system by primary afferent fibres. The two predominant classes of primary afferent fibres are small diameter Aδ fibers and C-fibers. Aδ fibers are thinly myelinated and are activated by mechanical and thermal nociception, while C-fibers are non-myelinated and are activated by high-intensity mechanical, chemical and thermal stimuli (Ohshiro *et al*. 2007). These axons carrying nociceptive information enter the spinal cord as dorsal roots through Lissauer's tract, and terminate mainly in laminae I and II of the dorsal horn and laminae V, VI, and X of the intermediate horn (Squire *et al*., 2003). The areas of the spinal cord associated with pain are illustrated in Figure 1. The rat lumbar spinal cord contains six segments, L1-L6, of which segments L2-L5 contain primary afferents supplying the hind limb (Hebel and Stromberg, 1986). Therefore, a nociceptive 15 V electrical stimulus applied to the hind paw of the rat should produce functional activation in the dorsal horn of lumbar spinal cord segments L2-L5.

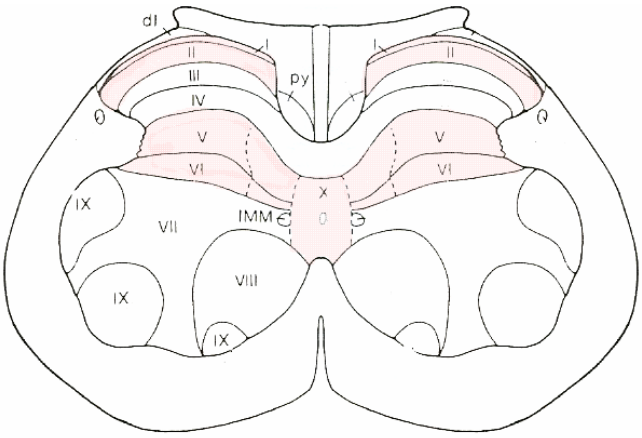

Figure 1. Schematic drawing of the lumbar spinal cord. Shaded areas indicate areas that are associated with pain. Laminae of Rexed indicated by roman numerals. Image was adapted from Molander and Grant (1995).

III.6. The hemodynamic response

Blood flow and energy metabolism are closely tied to neuronal activation (Gjedde, 2001). Upon neuronal excitation, blood flow increases to the nerve cell to supply oxygen for metabolism (Gjedde, 2001; Stroman *et. al*., 2005); however, oxygenated blood flow to the area of activation far exceeds metabolic need (Bandettini *et al*., 1997) and this increase in oxygenated blood in response to neuronal activation is called the hemodynamic response. FMRI is sensitive to the hemodynamic response to neuronal activation. Therefore, in response to a painful stimulus to the rat hind paw, the hemodynamic response should be detected by fMRI in areas of neuronal activity in the lumbar spinal cord, especially where primary afferent neurons synapse on second order neurons, primarily in laminae I and II.

III.7. Magnetic Resonance Imaging

Magnetic resonance uses the ability of nuclei with odd-numbered protons or neutrons to produce a magnetic moment when exposed to a magnetic field. In magnetic resonance imaging (MRI), the hydrogen nucleus (^{1}H) is typically used because its one proton gives a large magnetic moment and because it is very abundant in water throughout the body. The magnetic moment of hydrogen orients itself randomly in the absence of a magnetic field, but when it is exposed to a magnetic field, B_0, it aligns either parallel or anti-parallel to the field. The protons move about the B_0 in a specific manner known as precession.

The precessional frequency (ω_0) of a ^1H in a magnetic field of strength B_0 is given by the Larmor equation:

$$\omega_0 = B_0 \times \lambda$$

where λ is the gyromagnetic ratio, which is 42.577 MHz/T for a proton (Jezzard and Clare, 2001). Since there are more protons in the lower energy level (conventionally pointing up compared to down), there is a net magnetization vector produced. As field strength increases, more protons align with the field (Westbrook and Kaut, 1993). In order to see a signal in the MRI, the protons precessing in alignment with B_0 must be disturbed. A short radio frequency (RF) pulse applied at the same frequency as the precessing protons, the Larmor frequency, allows the protons to pick up energy from the radio wave; this is known as resonance. Therefore, at field strength of 7 Tesla, the precessional frequency of the applied RF pulse needs to be 298 MHz.

$$\varpi_0 = 7T \times 42.577 \frac{MHz}{T} = 298.04MHz$$

Applying an RF pulse at the same frequency as the precession frequency of the protons causes them to decrease the net longitudinal magnetization and increase their transversal magnetization as the protons start to precess in phase. Once the RF field is removed, the vector components begin to dephase and realign along B_0 and the absorbed energy is emitted. The time for recovery of longitudinal magnetization (T1) and the time for decay of transverse magnetization (T2) are different depending on the tissue type, and contribute to image contrast (Westbrook and Kaut, 1993). T2 decay, or spin-spin

relaxation, is due to interactions between neighbouring nuclei upon the removal of the RF pulse which causes them to dephase and reduce the net magnetization in the transverse plane, therefore reducing the voltage-induced signal produced at the receiver coil (Westbrook and Kaut, 1993). T1 and T2 have different values depending on the tissue type. Modifying the MR parameters can weight the images relative to T1 and T2 in order to optimize the image.

III.8. Functional Magnetic Resonance Imaging

In addition to T2 decay, rapid signal loss occurs when non-uniform local magnetic fields cause the protons to spin at different frequencies producing a faster loss of coherence (Westbrook and Kaut, 1993). A large source of magnetic field inhomogeneity comes from nuclei in the sample having very different magnetic susceptibilities, such as air/tissue interfaces or the level of deoxyhemoglobin in tissue near blood vessels (Jezzard and Clare, 2001). When hemoglobin has bound oxygen, it is diamagnetic and consequently produces little effect on the local magnetic field. However, in the absence of bound oxygen, hemoglobin is paramagnetic, producing a significant effect on the local magnetic field and decreasing the signal in the image (Jezzard and Clare, 2001). Oxygen is also paramagnetic, although the majority of oxygen in the blood is bound to hemoglobin so the effect of dissolved oxygen on the magnetic field is minimal, especially if the partial pressure of oxygen (pO_2) is kept within a normal physiological range. When there is a local increase in blood flow, the amount of oxyhemoglobin far exceeds the amount of deoxyhemoglobin in that area, and an increase in signal is seen because of the relative decrease in field distortion. This type of contrast is termed blood oxygenation

level dependent imaging (BOLD), which is dependent on the hemodynamic response function.

It is important to note that while the hemodynamic response is closely coupled to neuronal activity; it is an indirect measurement and has some limitations in temporal and spatial resolution. For example, while neuronal activation occurs on the millisecond time scale, the hemodynamic response occurs on a second time scale, peaking at about 6 s in the brain (Menon and Goodyear, 2001) and expected to be longer in the spinal cord (Stroman *et al*., 2002). For this reason, the stimulation paradigm can be designed to consist of alternating blocks of stimulation and resting conditions which occur over several seconds, since the response remains relatively constant throughout the time of stimulation (Bandettini *et al*., 1997). The hemodynamic response function can be convolved to fit the paradigm in the data analysis. Also, spatial resolution in fMRI is limited because there is likely to be a large signal due to blood flow response in the draining veins, and because signal is expected to appear over a larger area relative to the actual site of neuronal activity.

Gradient echo (GE) and spin-echo (SE) pulse sequences are sensitive to BOLD contrast and are typically used in fMRI. While GE sequences are more sensitive to the BOLD effect, spin echo sequences provide images with fewer artifacts (Jones *et al*., 2001). The spin echo sequence involves introducing a 180° RF pulse to refocus the spins in order to reduce field inhomogeneities and this is especially useful in the spinal cord, where CSF pulsation and bone/tissue interfaces contribute to field distortion.

In addition to the BOLD effect, Stroman *et al.* (2002; 2005) propose a second mechanism that contributes to the signal obtained in spin-echo fMRI termed signal enhancement by extravascular water protons (SEEP). SEEP contrast arises from a proton-density change due to an increase in perfusion pressure across blood vessels in response to neuronal activation. With the increase in perfusion pressure, water flows across vessel walls, thereby increasing the proton-density signal at that area. This increase in perfusion pressure is likely to occur in the vessels that are less flexible; indeed, Stroman *et al*. (2005) confirmed that the SEEP effect occurs largely in capillaries, arterioles and arteries, while the BOLD effect occurs predominantly in capillaries, venules and veins. With that in mind, by using a fast spin echo sequence that effectively combines both BOLD and SEEP effects, the signal obtained should reflect changes in oxyhemoglobin and deoxyhemoglobin that are most important at the level of the capillaries, which are closer to the "true" sites of neuronal activity.

The BOLD/SEEP activity was measured in the spinal cord of STZ-induced diabetic rats and healthy age-matched controls upon noxious electrical stimulus. Activity was expected in the dorsal horn ipsilateral to the site of stimulus, at the level of the lumbar enlargement. The fMRI activity in the spinal cord of diabetic and healthy control animals was compared in order to determine if there are detectable differences. Confirmation of differences in spinal cord fMRI activity between diabetic and control animals may be an indication that spinal fMRI can be a valuable tool in the early detection of diabetic neuropathy.

IV METHODS

IV.1. Animal preparation

Sixteen male Sprague-Dawley rats were obtained from the St. Boniface Research Centre, 8 of which had been confirmed STZ-induced diabetic for one month, and 8 were age matched control animals. Animals were treated according to the Canadian Council for Animal Care guidelines, and the protocol was approved by the IBD animal care committee. Each animal was anesthetized with isoflurane (3-4% induction, 1.5-2% maintenance) in a mixture of 40% oxygen and 60% nitrogen and intubated for mechanical ventilation (Columbus Instruments, Ohio, USA). Catheters (PE 50) were inserted in the left femoral artery so that arterial blood pressure and blood gases could be monitored, and in the left femoral vein for administration of α-chloralose anesthetic and fluids. Bupivacaine (0.25%) was administered to the wound site before suturing closed. After the surgery, the animal was transferred to the animal holder in the supine position, and isoflurane was discontinued as α-chloralose (30 mg/ml, 80 mg/kg) was administered over approximately 5 minutes. Maintenance doses of α-chloralose were administered (40 mg/ml) every 90 minutes or as required to counteract steep increases in blood pressure. Ventilation volume was adjusted in order to maintain normal arterial blood gases (pO_2 of 100-120 mmHg, pCO_2 of 35-45 mmHg) (Lawrence *et al*., 2004) while keeping the ventilation rate (58-60/minute) constant. Blood gases, pH, blood pressure, heart rate, and rectal temperature were monitored every ten minutes throughout the experiment to ensure a normal physiological range. Two small needle electrodes were placed subcutaneously on the right hind paw between the second and fourth digits and connected to a stimulation control box (IBD, Canada) that was triggered by the spectrometer to allow current from

the stimulator (Grass S48, Mass., USA) to either be delivered to the animal during the active stimulation condition (15 V, 0.3 ms duration, 3 Hz) or not be delivered during the resting condition. Prior to imaging, the stimulus was tested briefly to ensure that a toe twitch was observed. This ensures appropriate placement of the electrodes and that the stimulator is functioning appropriately. Following the fMRI experiments the animals were euthanized with pentobarbital (120 mg/kg, i.v.).

IV.2. Data acquisition

Images were acquired on a 7 T horizontal bore magnet and Avance console with 21 cm gradient insert (Bruker, Germany). The animal was placed supine in the animal holder so that the lumbar enlargement was centered over the surface coil. In order to correctly identify the lumbar enlargement, the animal was positioned with the 13th rib (which is attached to vertebra T13) located over the centre of the surface coil. The positioning was verified using scout images. The butterfly transmit and surface receive coil were tuned to 300 MHz. After shimming, scout images were acquired in axial and sagittal directions, using gradient echo sequences, to locate the lumbar spinal cord regions of interest. The thickest part of the spinal cord was used to landmark lumbar spinal cord segment L3, which is found between thoracic (T) vertebrae T12 and T13 (Hebel and Stromberg, 1986). The vertebrae above and below the thickest part were used to select slices corresponding to lumbar spinal cord segments L1 to L6 (Figure 2). Six 2 mm thick slices were chosen, spanning vertebrae T11/T12 to L1. FMRI experiments were conducted using a 2-shot fast spin-echo sequence (2 cm FOV, 128 x 64 matrix) with effective echo time of 54.6 ms and repetition time gated to respiration (approximately 3 s). Sixty time points were acquired using a block paradigm of six alternating rest and electrical

stimulation conditions (approximately 36 seconds per block, Figure 3). Each image was acquired in approximately 6 seconds, and the total acquisition time was approximately 6 minutes. The experiment was repeated three times for each animal, with 5 minutes rest between runs.

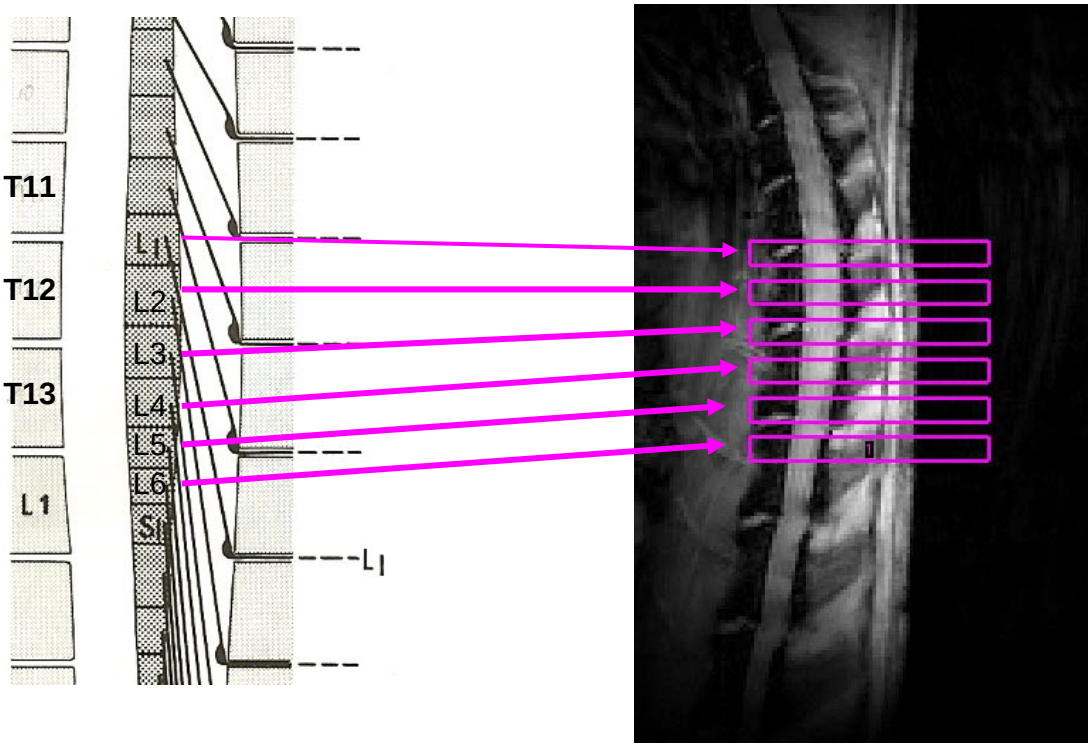

Figure 2. Anatomical image to identify lumbar spinal cord segments. The thickest part of the lumbar enlargement, located between vertebrae T12 and T13, was used to identify L3 and vertebrae above and below that landmark were used to identify segments L1-L6. Image on the left is adapted from Hebel and Stromberg (1986).

A noxious electrical stimulus (15 V, 0.3 ms duration, 3 Hz) was applied to the right hind paw, opposite the site of surgery. The electrical stimulus was tested outside of the magnet, and current was measured using an oscilloscope. A differential probe with a division ration of 1:20 and a 100 Ohm resistor were used to calculate the current,

$$I = \frac{V}{R} = \frac{V \times 20}{100}$$

where I is the current applied to the paw in mA, V is the measured voltage in mV, and R is the resistance in Ohm.

After the animal was killed, high-resolution T1-weighted images of the same six slices were acquired (128 x 128 matrix).

Figure 3. Stimulation paradigm. Electrical experiment block paradigm consisting of alternating resting and active stimulation conditions.

IV.3. Data analysis

A region of interest was selected around the spinal cord and data were analyzed by direct correlation on a pixel-by-pixel basis to the paradigm using custom-made software in IDL (Interactive Data Language, Research Systems Inc., Boulder, CO). A correlation coefficient of $R=0.333$ was used to give a $p \leq 0.01$. The activity maps generated for each of the three images for each animal were then combined and overlaid on the T1-weighted anatomical image using custom-made software developed in MatLab. These images were then manually overlaid using the same software to produce a combined activity map for each group. Signal intensity was graphed in a time course that is the convolution result of the hemodynamic response function and the stimulus paradigm. Time course data were averaged first for each animal then across control and diabetic groups. Statistical analysis was performed using a repeated measures analysis of variance (ANOVA), or an unpaired t-test, as appropriate. Differences were considered significant at the $p \leq 0.05$ level.

V. RESULTS

Diabetic animals were smaller, hyperglycemic, and had lower blood pH than control animals (Table 1). The diabetic rats seemed to be in much poorer health, indicated by severe diarrhea, which is expected by one month of uncontrolled STZ-induced diabetes. Blood gases (pO_2 and pCO_2) were maintained within normal physiological range throughout the fMRI experiments and averages for both groups are recorded in Table 1. One diabetic animal was excluded from the electrical stimulation experiment because of severe abdominal motion in response to the stimulus, and one control animal was excluded because of an error in data acquisition. The last three animals tested in both groups came from different batches of rats. The control rats from this batch did not respond with a noticeable twitch to the applied electrical stimulus. All other animals, including those in the second batch of diabetic rats, produced a clear twitch when the stimulus was turned on. This test is necessary to ensure appropriate application of the stimulus. Much greater voltage was required to be administered in order to confirm a toe twitch in the second batch of control rats. Similarly, the amount of signal change correlated to the stimulation paradigm was lower in these animals ($p=0.002$), and there was also much less activity in the fMRI images. The last three diabetic animals responded no differently to the electrical stimulus than the first batch of diabetic animals, with similar twitch response, percent signal change ($p=0.820$) and amount of activity in the fMRI images. The amount of current could not be measured in the second batch of animals due to a missing piece of equipment. Since the second batch of control rats responded very differently from the other control animals, it was not possible to assume that the applied current was the same. In addition, the lack of response in these animals

was abnormal and therefore the second batch of control and diabetic animals were both excluded from data analysis. The current applied to the paw in the first batch of animals was measured at 7.1 ± 0.9 mA. There was no difference between current measured in control animals and that measured in diabetic animals (p=0.332). The most common number of animals used in similar fMRI studies is 6 animals per group (Malisza *et al*., 2003; Lawrence *et al*., 2004, 2007, 2008; Majcher *et al*., 2006), however, statistical significance was still obtained between the two groups with only 4 animals per group in this experiment.

Table 1. Mean weight and some measured physiological parameters of the blood obtained during fMRI experiments in diabetic and control rats. (Mean ± SD)

Group	Weight (g)	Glucose (mmol/L)	pO_2 (mm Hg)	pCO_2 (mm Hg)	pH	Mean arterial pressure (mm Hg)
Diabetic (n=4)	367 ± 105 †	20 ± 3 *	118 ± 14	34 ± 7	7.3 ± 0.2 *	80 ± 13
Control (n=4)	527 ± 9	7 ± 2	109 ± 17	39 ± 6	7.47 ± 0.04	79 ± 17

† p<0.02
* p<0.005

V.1. Time course data

Active pixels that were correlated directly to the paradigm ($p \leq 0.01$) were assumed to be areas of neuronal activation in response to the applied stimulus. The percent signal change ($\Delta S/S \times 100$, where S is the baseline signal pre-stimulus and ΔS the change in signal during the stimulation condition) was averaged, first for the three experiments in each animal, then across each group, and plotted in Figure 4 (n=4/group). The time courses of signal obtained by fMRI closely follow the timing of the applied stimulus. Average signal change during stimulation periods ranged from 9% to 16%. The mean

signal change per stimulation condition was averaged for each animal then across animals in each group and plotted in Figure 5. A repeated measures analysis of variance (ANOVA) performed in Statistica (Statsoft, USA) on the five stimulation periods for control (n=4) and diabetic (n=4) animals indicates that the signal change is higher in control animals than in diabetics (p=0.027).

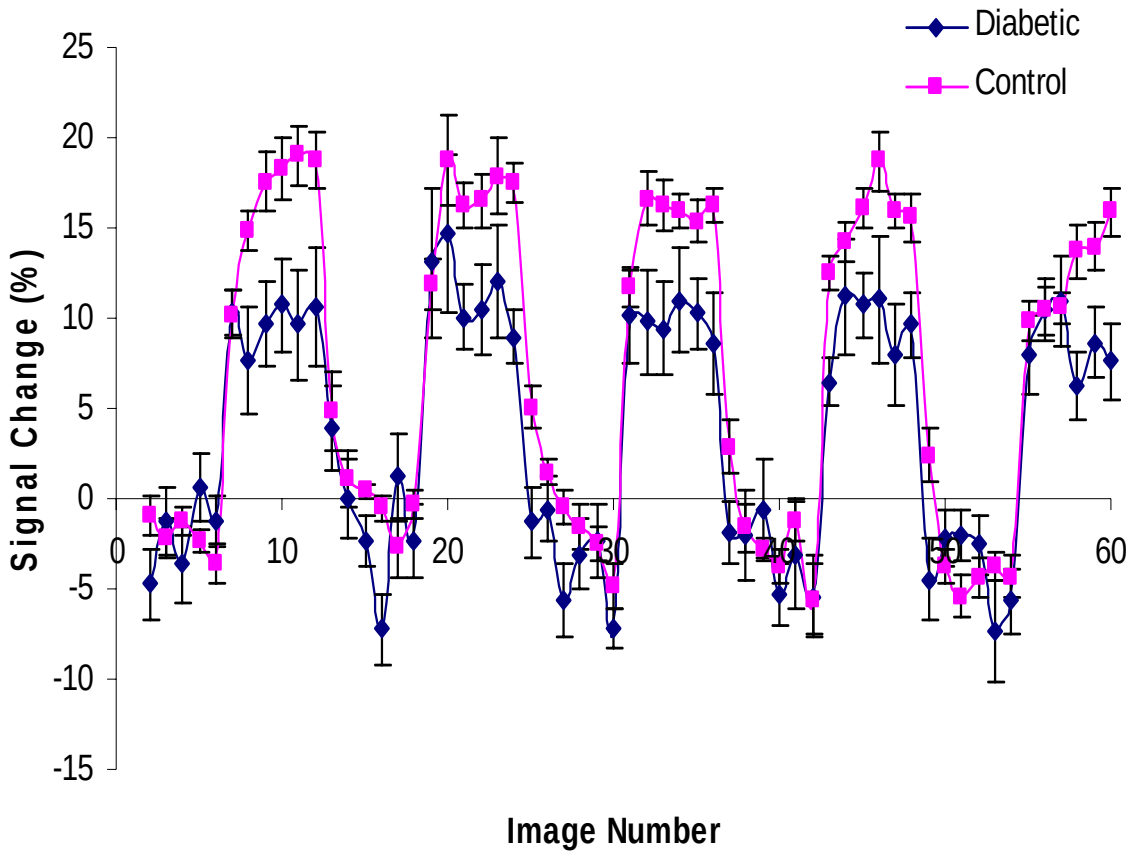

Figure 4. Averaged time courses of diabetic (n=4) and control (n=4) animals in response to noxious electrical stimulation. (mean ± SEM)

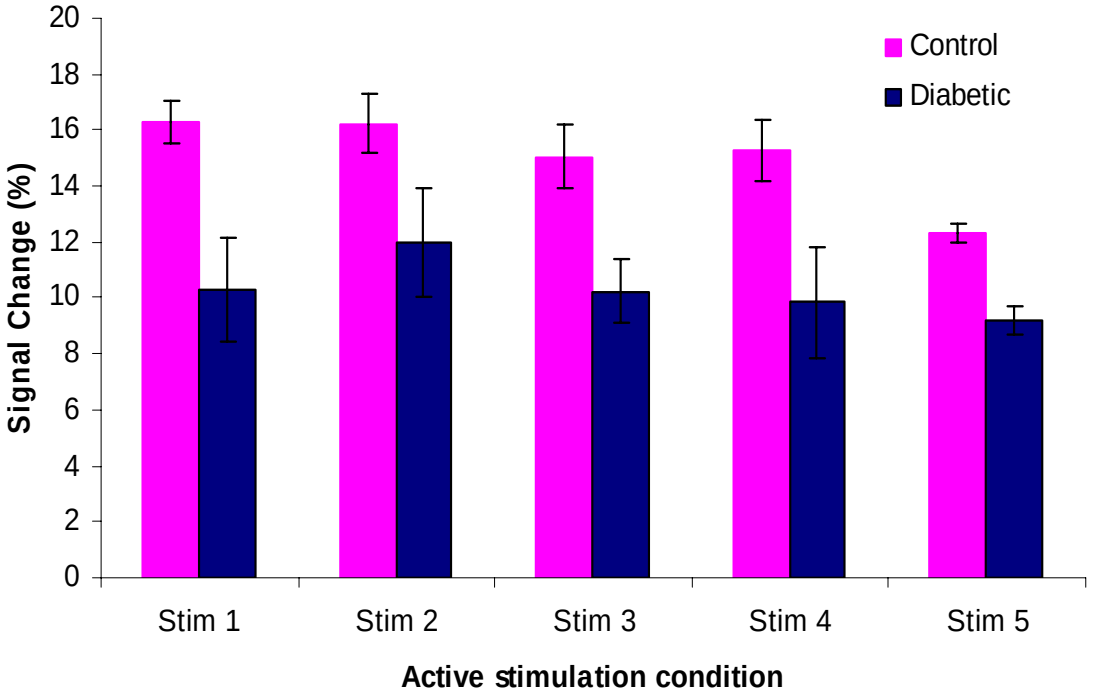

Figure 5. Mean signal intensity changes (mean ± SEM) across control (n=4, pink) and diabetic animals (n=4, blue) in each active stimulation period

V.2. Location of fMRI activity

In addition to greater percentage signal change in the control animals, more fMRI activity throughout the spinal cord was also observed. The fMRI activity was overlaid on a high resolution T1-weighted anatomical image for each animal. This is shown in Figure 6 for the control animals and Figure 7 for the diabetic animals. High resolution images could not be acquired for the correct fMRI slices in two animals (diabetic animals 2 and 5). These fMRI images were overlaid on anatomical images of different animals whose spinal cord areas for each slice were of similar size (diabetic animals 6 and 3). A combined activation map for each group was then prepared by overlaying activity maps for each of the 4 animals used in the data analysis (Figure 8). Consistent fMRI activity was observed in the dorsal horn ipsilateral to the site of stimulus (right side), in control rats at spinal cord segments L2 to L5, and in the diabetic rats at segments L1 to L4.

Significantly greater activity was observed in the control animals in the dorsal horn contralateral to the site of stimulus (left side) at segments L1 to L4, and in both ipsilateral and contralateral ventral horn. Activations located central to and above the grey matter were observed in both control and diabetic animals.

In order to ensure that the orientation of the images was correct and not flipped at some point in the data analysis, a small tube filled with dilute copper sulfate was placed under one animal on the right side, and functional images were obtained. The bright circle corresponding to the copper sulfate-filled tube was located on the right side of the image after data analysis, indicating that the right side of the image does correspond to the right side of the animal.

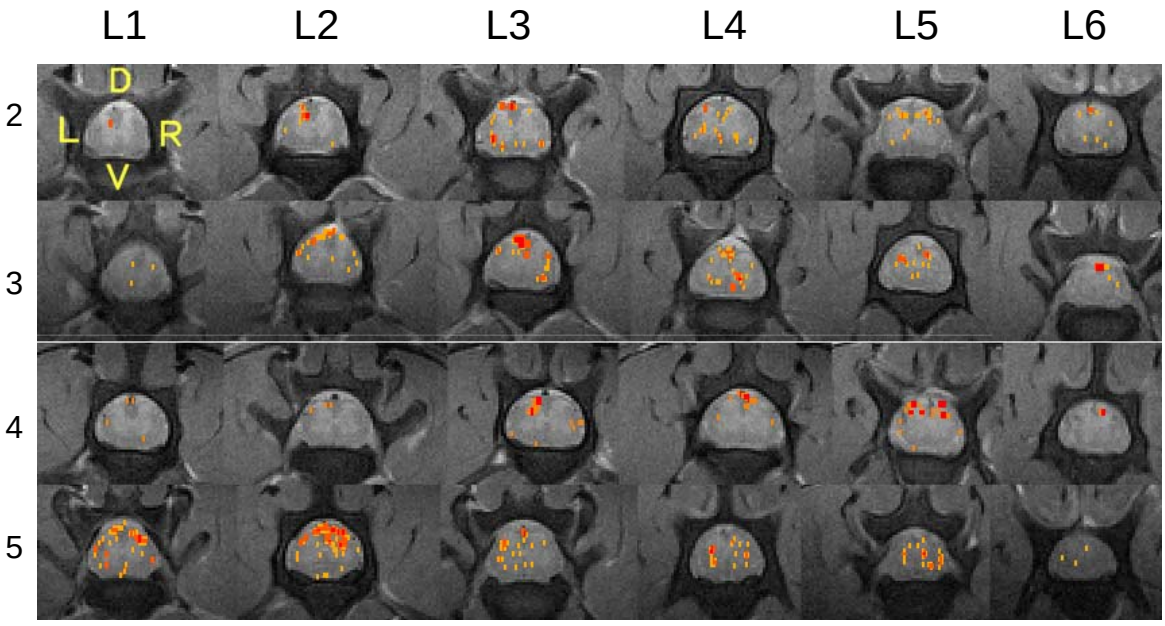

Figure 6. fMRI activation map in control animals following noxious electrical stimulation of the right hind paw. Red colour indicates overlap between all electrical experiments for that animal, whereas lighter colour indicates activation in one experiment only. Active pixels were directly correlated to the paradigm at a threshold of $p \leq 0.01$. R: Right; L: Left; D: Dorsal; V: Ventral; only first batch of animals shown

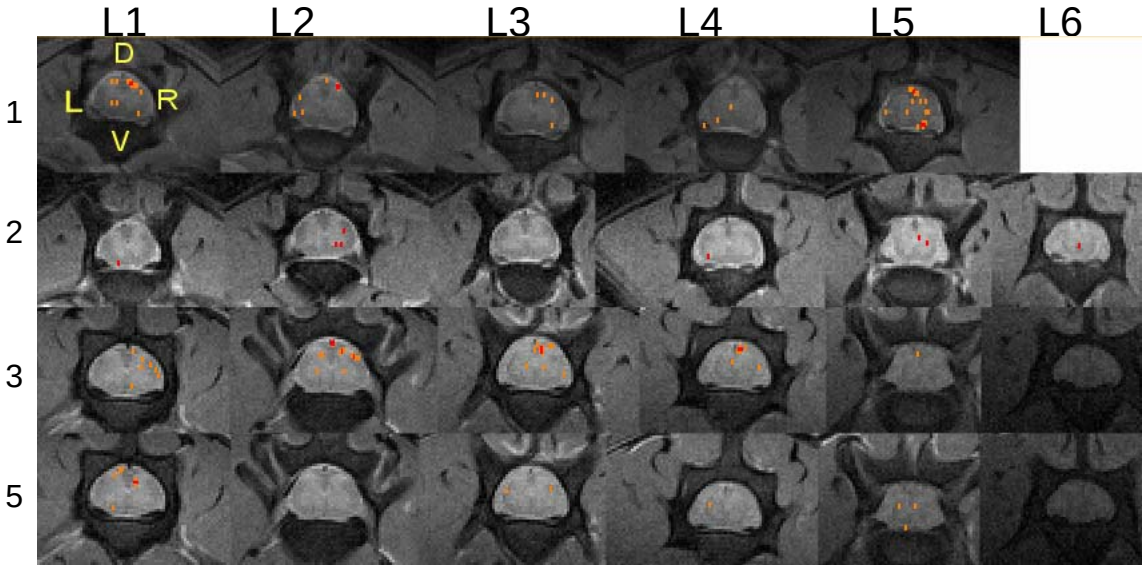

Figure 7. fMRI activation map in diabetic animals following noxious electrical stimulation of the right hind paw. Red colour indicates overlap between all electrical experiments for that animal, whereas lighter colour indicates activation in one experiment only. Active pixels were directly correlated to the paradigm at a threshold of $p \leq 0.01$. R: Right; L: Left; D: Dorsal; V: Ventral; only first batch of animals shown.

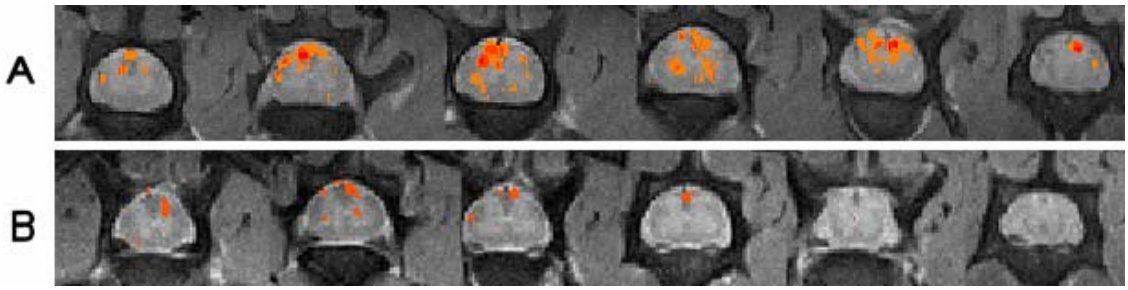

Figure 8. Overlay of combined fMRI activations in A) control animals (n=4) and B) diabetic animals (n=4) during noxious electrical stimulation of the right hind paw. Single pixels were removed so that only areas containing at least 2 overlapped pixels are displayed. Darker red colour indicates areas of greater overlap.

VI. DISCUSSION

In this study, I used a fast spin-echo sequence to detect fMRI activation in the lumbar enlargement of the spinal cord in response to noxious electrical stimulation of the hind paw. As expected, all animals displayed activity in the dorsal horn ipsilateral to the site of stimulus, which is consistent with other studies involving noxious electrical stimulation of a hind limb using FSE (Lawrence *et al*., 2004) and GE sequences (Lilija *et al*., 2006; Zhao *et al*., 2007). Control animals displayed much more activity throughout the spinal cord, including the dorsal horn contralateral to the site of stimulus and in the ventral horn both contralateral and ipsilateral to the applied stimulus. The ipsilateral ventral horn activity is likely due to a reflex response and is consistent with similar fMRI studies (Lawrence *et al*., 2004; 2007; 2008; Majcher *et al*., 2006; Malisza *et al*. 2003). Some studies use the muscle relaxant, pancuronium bromide, to reduce motion, and in these studies the apparent activity in the ventral horn ipsilateral to stimulus is reduced (Lilija *et al*., 2006; Majcher *et al*., 2006; Zhao *et al*., 2007). I did not use pancuronium in this study. There did not appear to be a great deal of motion artifacts in the individual images, so I assume that apparent activation due to motion is minimal. The activations observed in other areas of the grey matter may be due to communication between neurons, as axons carrying nociceptive information can synapse on interneurons involved in the arc reflex or on other neurons involved in ascending pathways. The activity located central to and above the grey matter of the spinal cord in both groups of animals is likely due to the dorsal spinal vein. The dorsal spinal vein is located above the spinal cord and outside the region of interest, but since it is a major draining vein that is very close to the spinal cord,

it is expected to exhibit a large increase in blood oxygenation, which may cause fMRI signal to be seen in nearby regions.

The amount of signal change for control animals is similar in comparison to other fMRI studies using alpha-chloralose anesthesia and a fast spin echo sequence at 7 T (Lawrence *et al*., 2004; 2007; 2008) as well as at 9.4 T (Malisza *et al*., 2003). However, the percentage signal change was higher in this experiment than in one performed at 9.4 T (Majcher *et al*., 2006). This discrepancy is likely due to differences in experimental setup, depth of anesthesia, and method of data analysis.

At one month post-injection, STZ-induced diabetic rats exhibit an exaggerated response to painful stimuli (Gabra *et al*., 2006). It is therefore somewhat surprising that the results of this study indicate that there is less fMRI activity in the dorsal horn of diabetic rats in response to a painful stimulus, as indicated by a smaller percentage signal change. In general, the amount of signal change in fMRI is thought to be related to the number of neurons firing. Therefore, the decreased contralateral activity may be interpreted as diminished communication between neurons within the spinal cord, and the reduced activity in the dorsal horn the result of fewer recruited primary afferent neurons. However, there is no significant axonal degeneration in this model of diabetes at one month (Mizicin *et al.*, 2007). Consequently, the observation that diabetic animals have much less fMRI activity in the spinal cord and smaller percentage signal change may not be the result of fewer recruited primary afferent neurons but may involve either reduced communication between primary and secondary neurons or other factors influencing the

hemodynamic response. Since fMRI is not a direct measure of neuronal activity, but is a measure of the hemodynamic response to neuronal activation, factors affecting the hemodynamic response in diabetic rats may play a role in the fMRI signal obtained.

There are some vascular complications in diabetes that may contribute to the difference in hemodynamic response, such as reduced blood flow and ischemia. Endoneurial blood flow (NBF) is reduced in diabetes, which is thought to be due to increased blood viscosity and altered vasoregulation of microvessels (Low *et al*., 1999). It is likely that blood flow within the spinal cord itself may also be reduced, however, I am unaware of any studies that involve blood flow measurement within the spinal cord in diabetes. Should blood flow in the spinal cord of diabetic rats be reduced compared to controls, this may have an effect on the amount of signal obtained in the spinal cord in fMRI. Thus, a lower percentage signal change in fMRI of the spinal cord in diabetic rats may be partly explained by reduced blood flow. Another related factor that may influence the BOLD signal is ischemia because the resulting hypoxia might reduce the amount of oxygenated hemoglobin that could be measured. In this experiment, hypoxia does not play a large role in the difference in signal because blood gases were monitored and the ventilation rate was adjusted to ensure that arterial oxygen was consistent throughout the studies in both diabetic and control animals.

In a study on fMRI of the rat spinal cord in response to electrical stimulation, Zhao *et al*. (2007) propose that the vasodilator peptide, substance P, in the spinal cord may contribute to the signal obtained by BOLD fMRI by increasing local blood flow and

volume. The reduction in percentage signal change in diabetic rats may therefore be due to a reduced level of substance P upon noxious stimulation. This is consistent with reports that, while diabetic rodents exhibit an exaggerated nociceptive response, they do so with reduced input from primary afferent fibers to the spinal cord (Calcutt, 1999). Neurochemical studies have shown that substance P and calcitonin gene related peptide (CGRP) release in sensory ganglia (Calcutt *et al*., 1990; Apfel *et al*., 1994; Fernyhough *et al*., 1995) and substance P release in spinal dialysates (Calcutt *et al*., 1999) is lower in diabetic animals than in control animals. In addition, nerve growth factor administered to diabetic rats restores the normal level of substance P and CGRP release (Apfel *et al*., 1994; Fernyhough *et al*., 1995). Substance P and CGRP are found in both unmyelinated and thinly myelinated fibers that terminate in laminae I and II (Ribeiro-da-Silva, 1995), although Zhao *et al*. (2007) suggests that substance P is only released from unmyelinated C-fibers. The electrical stimulus that was used is likely to activate both C- and A-fibers, although a previous study showed that only C-fiber stimulation produced detectable fMRI activity (Zhao *et al*., 2007). Therefore, the fMRI activity that was observed is likely the result of C-fiber stimulation. The vasoactive peptides released from C-fibers, substance P and CGRP, may increase the BOLD signal. It is possible that the smaller fMRI signal obtained in the lumbar spinal cord of diabetic rats is in part due to the reduced levels of substance P and CGRP, though more investigation on the effect of these peptides on the fMRI signal is needed.

While the hemodynamic response in fMRI studies of the brain is well established, spinal fMRI is a relatively new technique. The reasons accounting for differences in signal

intensity between brain and spinal fMRI have yet to be firmly established. Differences in anatomy, vasculature, and neurochemistry may all contribute to the fMRI signal. Several technical issues make fMRI of the spinal cord particularly challenging. For example, vasculature, cerebral spinal fluid (CSF) pulsation, motion, and magnetic field distortions due to tissue interfaces may decrease signal to noise ratio. Although the arteries supplying the spinal cord and the veins draining the spinal cord are exterior to the cord, weaker signal coming from the interior may be obscured by the signal from larger vessels (Giove *et al*., 2004). In an effort to reduce the amount of noise due to vasculature, I drew a region of interest containing only the spinal cord when performing the data analysis. Motion artifacts also present a challenge in Spinal fMRI, because of the motion of the CSF, the proximity of the lungs (mainly when imaging the cervical spine), and the movement of spinal cord itself. The CSF, which bathes the spinal cord, and is in the central canal, pulses with the cardiac and respiratory cycles (Giove *et al*., 2004). Because the signal from this kind of motion is based on physiological rhythms, and not correlated to the paradigm, I would expect that at a correlation threshold of $p<0.01$ the motion artifacts contributed by CSF flow would be minimal. A more prominent motion artifact may come from motion of the spinal cord itself, as this might occur as a response to the applied stimulus. If the rat were to jump or twitch in response to the applied electrical current, it is possible for movement of the spinal cord to occur, producing motion artifacts in the cord. In this experiment, the animals did not appear to move once they were under anesthetic, however, once they are inside the bore of the magnet it is impossible to judge whether they are moving or not. The small twitch produced by the electrical stimulus is not likely to produce movement within the spinal cord itself.

However, the diabetic animals sometimes exhibited some random peristaltic movement in the abdomen, which might contribute to spinal cord movement not correlated to the paradigm. In order to reduce the motion due to respiration, the MR acquisition was gated to the respiratory cycle. The lumbar spine is not likely to be as sensitive to this type of movement as are cervical and thoracic segments because it is farther from the lungs. Finally, susceptibility artifacts due to tissue interfaces are particularly important in the spinal cord due to the many different types of tissues in the spinal cord area. In particular, bone/tissue interfaces produce these artifacts leading to field inhomogeneities (Giove *et al*., 2004). Giove *et al*. (2004) suggest selecting slices that are either completely within vertebrae or completely between vertebrae in order to minimize the tissue interfaces between bone and connective tissue, however, this advice is directed towards imaging the human spinal cord and is not very practical with a small animal such as the rat, since vertebrae are very small and it would require decreasing the slice thickness to less than 2 mm, although I did try as much as possible to centre the slices on the vertebra and intervertebral discs.

In addition to these issues with spinal fMRI, there is also a challenge in imaging small animals. The 7 T magnet I used was not intended for small animals. A gradient insert was used in order to decrease the field of view to a size appropriate for imaging the spinal cord of the rat. While gradient inserts have been used in several other studies involving fMRI of the spinal cord in rodents (Lawrence *et al*., 2004; 2007; 2008), it is possible that the signal to noise ratio could be reduced by using a dedicated small animal system.

In this experiment, there is some variation between animals in the percentage signal change in response to stimulation, with greater variation occurring in the diabetic animals. Variation between animals is expected, and can be attributed to a variety of factors, including depth of anesthesia, each animal's sensitivity to the stimulus and physiology, MRI system instability between experiments, and variation in the slice position (Majcher *et al*., 2006). In addition to variability between animals, there was also a great amount of variability between animal litters. Since I could not measure the current in the second batch of rats, it is hard to say whether the smaller toe twitch outside of the magnet was due to differences in physiology or a problem in delivering the same amount of current. Even with the same amount of applied voltage to these animals as in the first batch of animals, the response, in terms of fMRI activity and percentage signal change, was greatly reduced. In order to minimize the differences in stimulus strength across animals, the amount of current measured in the animal, as opposed to the applied voltage, should be kept constant. In this experiment, I kept the voltage constant rather than the measured current. Since the current that was measured in the two first groups is relatively constant, this was not an issue, but future experiments should involve using a stimulus with constant current. However, given previous experience applying this electrical stimulus to the rat paw (N≈50), the response of this second batch of control animals was not normal. Even without knowing the current, placement of the electrodes just under the skin and applying 15 V should produce a visible toe twitch. It is likely that there was a problem with the second batch of controls.

The larger differences in signal intensity between diabetic animals might be explained by a greater degree of variation in disease state. To minimize differences between diabetic rats, the STZ-induced animals should be selected based on a minimum level of allodynia. This can be measured behaviourally by pressing Von Frey hairs of varying weights against the foot of the rat in order to provoke a withdrawal response. A 50% withdrawal threshold to weights of less than 5 g can be considered allodynic (Chaplan *et al*., 1994).

Despite variation between animals, it is clear that there are differences between groups of diabetic and control rats that can be detected by fMRI in the lumbar spinal cord. Diabetic animals had lower percentage signal change as well as fewer fMRI activations in the spinal cord at the level of the lumbar enlargement in response to noxious electrical stimulation of the hind limb. These results are promising in that they indicate potential for using fMRI as a tool for early detection of diabetic neuropathy.

VII CONCLUSIONS

1. STZ-induced diabetic rats, that were diabetic for one month, were smaller, hyperglycaemic, and had a lower blood pH than healthy age-matched control rats.

2. Diabetic rats exhibited lower percentage signal change in the spinal cord at the lumbar enlargement in response to noxious electrical stimulation of the hind paw.

3. Both control and diabetic rats displayed fMRI activity at the level of the lumbar enlargement in the dorsal horn ipsilateral to the site of painful electrical stimulus, supporting my hypothesis.

4. Control rats demonstrated greater fMRI activity during electrical stimulation in the contralateral dorsal horn as well as in both contralateral and ipsilateral ventral horns.

VIII REFERENCES

Apfel, S.C., Arezzo, J.C., Brownlee, M., Federoff, H., and J.A. Kessler. 1994. Nerve growth factor administration protects against experimental diabetic sensory neuropathy. Brain research 634: 7-12

Bandettini, P., Kwong, K., Davis, T., Tootell, R., Wong, E. Fox, P., Weisskoff, R., and B. Rosen. 1997. Characterization of cerebral blood oxygenation and flow changes during prolonged brain activation. Human brain mapping 5:93-109.

Calcutt, N.A., Tomlinson, D.R., Willars, G.B., and P. Keen. 1990. Axonal transport of substance P-like immunoreactivity in ganglioside-treated diabetic rats. Journal of neurological science. 96:283-291

Calcutt, N and S. Chaplan. 1997. Spinal pharmacology of tactile allodynia in diabetic rats. British journal of pharmacology 122: 1478-1482

Calcutt, N.A., Stiller, C., Gustafsson, H., and A.B. Malmberg. 1999. Elevated substance-P-like immunoreactivity levels in spinal dialysates during the formalin test in normal and diabetic rats. Brain Research 856: 20-27

Ceseña RM, and N.A. Calcutt. 1999. Gabapentin prevents hyperalgesia during the formalin test in diabetic rats. Neuroscience letters. 262: 101-104.

Chaplan, S.R., Bach, F.W., Pogrel, J.W., Chung, J.M., and T.L. Yaksh. 1994. Quantitative assessment of tactile allodynia in the rat paw. Journal of neuroscience methods. 53: 55-63

Ekström P.A.R., and D.R. Tomlinson. 1989. Impaired nerve regeneration in streptozotocin-diabetic rats: effects of treatment with an aldose reductase inhibitor. Journal of neurological science. 93:231-237.

Fernyhough P, Diemel L.T., Hardy J, Brewster W.J., Mohiuddin L, and D.R. Tomlinson. 1995. Human recombinant nerve growth factor replaces deficient neurotrophic support in the diabetic rat. European journal of neuroscience. 7: 1107-1110.

Freshwater, J.D., Svensson, C.I., Malmburg, A.B., and N.A. Calcutt. 2002. Elevated spinal cyclooxygenase and prostaglandin release during hyperalgesia in diabetic rats. Diabetes. 51: 2249-2255

Freshwater, J. and N.A. Calcutt. 2005. Low doses of formalin reveal allodynia in diabetic rats. Journal of neuropathic pain and symptom palliation. 1: 39-46

Gabra, B.H., Berthiaume, N., Sirois, P., Nantel, F., and B. Battistini. 2006. The kinin system mediates hyperalgesia through the inducible bradykinin B1 receptor subtype: evidence in various experimental animal models of type 1 and type 2 diabetic neuropathy. Biological chemistry. 387:127-143

Giove, F., Garreffa, G., Mangia, S., Colonnese, C., and B. Maraviglia. 2004. Issues about the fMRI of the human spinal cord. Magnetic resonance imaging 22: 1505-1516

Gjedde, A. 2001. Brain energy metabolism and the physiological basis of the haemodynamic response. In: Jezzard, P., Matthews, P.M., and Smith, S.M., editors. Functional MRI: an introduction to methods. Oxford: University press. p 37-65

Hebel, R. and M. Stromberg. 1986. Anatomy and embryology of the laboratory rat. Worthsee, Germany: Biomed Verlag. p 124-132

Honda, K., Koguchi, M., Nakajima, K., Kobayashi, F., Migita, K., Ogata, S., Hirabara, Y. and Y. Takano. 2007. Contribution of Ca2+-dependent protein kinase C in the spinal cord to the development of mechanical allodynia in diabetic mice. Biological and pharmaceutical bulletin. 30(5):990-993

Jezzard, P. and S. Clare. 2001. Principles of nuclear magnetic resonance and MRI. In: Jezzard, P., Matthews, P.M., and Smith, S.M., editors. Functional MRI: an introduction to methods. Oxford: University press. p 67-92

Jones, R., Brookes, J. and C. Moonen. 2001. Ultra-fast fMRI**.** In: Jezzard, P., Matthews, P.M., and Smith, S.M., editors. Functional MRI: an introduction to methods. Oxford: University press. p 93-108

Lawrence, J., Stroman, P.W., Bascaramurty, S., Jordan, L.M., and K.L. Malisza. 2004. Correlation of functional activation in the rat spinal cord with neuronal activation detected by immunohistochemistry. Neuroimage. 22: 1802-1807

Lawrence, J., Stroman, P.W., and K.L. Malisza. 2007. Comparison of functional activity in the rat cervical spinal cord during alpha-chloralose and halothane anesthesia. Neuroimage. 34: 1665-1672

Lawrence, J., Stroman, P.W., and K.L. Malisza. 2008. Functional MRI of the cervical spinal cord during noxious and innocuous thermal stimulation in the a-chloralose- and halothane-anesthetized rat. Magnetic resonance imaging. 26: 1-10

Lilija, J., Endo, T., Hofstetter, C., Westman, E., Young, J., Olson, L., and C. Spenger. Blood oxygenation level-dependent visualization of synaptic relay stations of sensory pathways along the neuroaxis in response to graded sensory stimulation of a limb. The journal of neuroscience. 26: 6330-6336

Low, P.A., Nickander, K.K., and L. Scionti. 1999. Role of hypoxia, oxidative stress, and excitatory neurotoxins in diabetic neuropathy. In: Dyck, P.J. and Thomas, P.K, editors. Diabetic neuropathy, 2nd Ed. Philadelphia: W.B. Saunders Company. p 317-329

Majcher, K., Tomanek, B., Jasinski, A., Foniok, T., Stroman, P.W., Tuor, U.I., Kirk, D., and G. Hess. 2006. Simultaneous functional magnetic resonance imaging in the rat spinal cord and brain. Experimental neurology. 197:458-464

Malisza, K.L. and P.W. Stroman. 2002. Functional imaging of the rat cervical spinal cord. Journal of magnetic resonance imaging. 16: 553-558.

Malisza, K.L., Stroman, P., Turner, A., Foniok, T., Gregorash, L. and A. Wright. 2003. Functional MRI of the rat lumbar spinal cord involving painful stimulation and the effect of peripheral joint mobilization. Journal of magnetic resonance imaging. 18:152-159

Menon, R.S. and B.G. Goodyear. 2001. Spatial and temporal resolution in fMRI**.** In: Jezzard, P., Matthews, P.M., and Smith, S.M., editors. Functional MRI: an introduction to methods. Oxford: University press**.** p 146-158

Mizicin, A., Jolivalt, C.G., and N.A. Calcutt. 2007. Spinal cord structure and function in diabetes. In: Veves, A., and Malik, R., editors. Contemporary diabetes: diabetic neuropathy: clinical management, 2nd ed. NJ: Humana Press Inc. p 165-185.

Molander, C. and G. Grant. 1995. Spinal cord cytoarchitecture. In: Paxinos, G., editor. The rat nervous system, 2nd ed. CA: Academic Press. p 42.

Ohshiro, H., Ogawa, S. and K. Shinjo. 2007. Visualizing sensory transmission between dorsal root ganglion and dorsal horn neurons in co-culture with calcium imaging. Journal of neurosciences methods 165: 49-54

Ramos, K., Jiang, Y., Svensson, C., and N. Calcutt. 2007. Pathogenesis of spinally mediated hyperalgesia in diabetes. Diabetes. 56:1569-1576

Ribeiro-da-Silva, A., 1995. Substantia gelatinosa of spinal cord. In: Paxinos, G., editor. The rat nervous system, 2nd Ed. Sydney: Academic press. p 52-53

Scott, L. and S. Tesfaye. 2001. Measurement of somatic neuropathy for clinical practice and clinical trials. Current diabetes reports. 1:208-215

Selvarajah, D., Wilkinson, I., Emery, C., Harris, N., Shaw, P., Witte, D., Griffiths, P., and S. Tesfaye. 2006. Early involvement of the spinal cord in diabetic peripheral neuropathy. Diabetes care. 29:2664-2669

Squire, L., Bloom, F., McConnell, S., Roberts, J., Spitzer, N. and M. Zigmond. 2003. Fundamental Neuroscience. 2nd Ed. USA: Academic Press. 667-682

Stroman, P.W., Tomanek, B., Krause, V., Frankenstein, U.N., and K.L. Malisza. 2002. Mapping of neuronal function in the healthy and injured human spinal cord with spinal fMRI. Neuroimage. 17: 1854-1860.

Stroman, P.W., Kornelson, J., Lawrence, J., and K.L. Malisza. 2005. Functional magnetic resonance imaging based on SEEP contrast: response function and anatomical specificity. Magnetic resonance imaging. 23: 843-850

Tomlinson, D.R., Holmes, P.R., and J.H. Mayer. 1982. Reversal, by treatment with an aldose reductase inhibitor, of impaired axonal transport and motor nerve conduction velocity in experimental diabetes mellitus. Neuroscience letters. 31: 189-93.

Westbrook, C. and Kaut, C. (1993) MRI in practice. Oxford: Blackwell scientific publications

World Health Organization. 1998. The World Health Report 1998: Life in the 21st Century: a vision for all. 1-241

Zhao, F., Williams, M., Meng, X., Welsh, D., Coimbra, A., Crown, E.D., Cook, J.J., Urban, M.O., Hargreaves, R., and D.S. Williams. 2007. BOLD and blood volume-weighted fMRI of rat lumbar spinal cord during non-noxious and noxious electrical hindpaw stimulation. Neuroimage. doi:10.1016/j.neuroimage.2007.11.010